Supporting Information

Markus Joos[a], Maurice Conrad[b,c], Igor Moudrakovski[a], Maxwell W. Terban[a], Ashkan Rad[a], Payam Kaghazchi[d], Rotraut Merkle*[a], Robert E. Dinnebier[a], Thomas Schleid[b], and Joachim Maier[a]

a Max Planck Institute for Solid State Research, Heisenbergstr. 1, 70569 Stuttgart, Germany.

b Institut für Anorganische Chemie, University of Stuttgart, Pfaffenwaldring 55, 70569 Stuttgart, Germany.

c (present address) Institut für Photovoltaik, University of Stuttgart, Pfaffenwaldring 47, 70569 Stuttgart, Germany.

d Forschungszentrum Jülich GmbH, Institute of Energy and Climate Research, Materials Synthesis and Processing (IEK-1), 52425 Jülich, Germany.

*Corresponding author Email: r.merkle@fkf.mpg.de

Experimental

General

All preparation and measurement conditions were the same as reported in Part I[1] of this series. Syntheses, sample preparation methods and material characterizations are described in the Supporting Information of Part I[1] and can be reviewed there. Any additional preparation method or measurement technique in this report is shown hereafter.

Spark Plasma Sintering (SPS)

Spark plasma sintering (HP D 5 SPS, *FCT Systems GmbH*, Germany) of 500 mg of dry Li(SCN) in a 10 mm graphite die produced fully densified pellets (up to 95% density), applying a force of 8 kN (1 kbar) and heating to 240 °C for 1 min (heating and cooling rate 20 K/min). The Li(SCN) powder and resulting pellet were exposed to air for ~30 s during transfer steps. Thereafter, the pellet was cleaned with SiC paper and polished with Al_2O_3 (9MIC, 3M *Lapping Film*) lapping paper in a glove box.

^{15}N enrichment of Li(SCN)

Commercially available ^{15}N enriched K(SCN) (98 at.-% ^{15}N, *Sigma-Aldrich*, Steinheim, Germany) was converted into ^{15}N enriched Li(SCN) by means of cation exchange applying a method similar to a literature procedure.[2] A column filled with the cation-exchange resin Amberlite® IR-120 (*Fluka*, Buchs, Switzerland) in its H^+ form was quantitatively loaded with Li^+ cations by passing through a solution of lithium chloride (LiCl: p.a., *CARL Roth*, Karlsruhe, Germany). Afterwards, the column was flushed with demineralized water to remove Cl^- anions. A 0.05 M solution of silver nitrate ($Ag(NO_3)$: 99,5%, *Grüssing GmbH*, Filsum, Germany) was used to catch the passed through solution and indicate the absence of Cl^- anions. Afterwards, an aqueous solution of ^{15}N enriched K(SCN) was run through the column. The

resulting solution of ^{15}N enriched Li(SCN) was evaporated under reduced pressure until only a few millilitres remained and subsequently transferred into a Schlenk flask. After drying the sample for a few hours at room temperature and consequently for 48 hours at 200-250 °C in a dynamic vacuum, a white hygroscopic solid of ^{15}N enriched Li(SCN) was formed.

Solid State Nuclear Magnetic Resonance (ssNMR)

ssNMR measurements were conducted with powdered samples of Li(SCN), which for sensitivity improvement were compacted by uniaxial cold pressing (4 mm diameter, 10 kN (8 bar)). Several pellets to a filling height of $\leq$ 35 mm were inserted under argon into a 5 mm outer diameter NMR glass tube (*Deutero*), equipped with a ground glass joint for evacuation. The samples were flame sealed under light static vacuum (< 0.5 bar). Spectra were acquired on a *Bruker* Avance III 400 MHz instrument (magnetic field of 9.4 T) at Larmor frequencies of 155.5 MHz (^{7}Li), 58.8 MHz (^{6}Li) and 40.6 MHz (^{15}N), using a *Bruker* static double resonance PE400 probe with a horizontal 5 mm coil. Between 8 and 64 scans were commonly averaged for a good signal-to-noise ratio. In addition, magic angle spinning (MAS) measurements were recorded using a *Bruker* BL4 double resonance MAS probe and 4 mm outer diameter ZrO_2 spinners. For MAS measurements, the powders of studied materials were flame sealed in fitted 3 mm outer diameter pyrex MAS inserts for *Bruker* 4 mm rotors (*Wilmad Glass*, product #DWGSK2576-1). The MAS spectra for all nuclei were acquired with a simple Bloch decay experiment (pulse-acquisition), with acquisition delays set sufficiently long for a complete magnetization recovery. The ^{7}Li static experiments were performed using solid-echo with central transition selective 90° pulses (the non-selective liquid 90° pulses were scaled by a factor of (I + 0.5) – 1 = 0.5).[3,4] All spin-lattice relaxation time measurements used the saturation-recovery method with 8-16 recovery delays. [47,48] The temperature in the probes was regulated with a *Bruker* BVT3000 temperature controller. Actual temperature of the sample was calibrated on ^{207}Pb signal of powdered $Pb(NO_3)_2$.[5] Chemical shifts were referenced externally relative to 1 M LiCl (^{6,7}Li, δ_{iso} = 0.0 ppm) and liquid $CH_3(NO_3)$ (^{15}N, δ_{iso} = 0.0 ppm).[6]

Electrochemical Impedance Spectroscopy (EIS)

The same sample preparation method, measurement conditions and instrumental set-up for EIS as reported in Part I[1] was also used in this work. While in part I we focused on long-range transport only (extracting the conductivity from the lower frequency part of the bulk response), we now investigate the frequency dependence of bulk ion transport (best visible in modulus representation, cf. Figure 1b and S5) in more detail. For Figure 2a the spectra are fitted with the circuit shown in Figure 1a, and the conductivities of the high (ω_1) and low (ω_2) frequency process of bulk transport calculated from it. In addition, the instrumental uncertainty at high frequencies was assessed using an appropriate test circuit (Ser $\{\mathrm{Par}[3\ \mathrm{M\Omega},\ 10\ \mathrm{pF}],\ \mathrm{Par}[1.5\ \mathrm{G\Omega},\ 10\ \mathrm{pF}]\}$) as reference. A sample of lithium iodide (LiI: *Sigma Aldrich*) was measured to compare its impedance response with Li(SCN). It was first dried at 300 °C under dynamic vacuum of a Schlenk line ($p \leq 10^{-2}$ mbar). The pellet was cold pressed and

sputtered as described for Li(SCN) in Part I (relative density 94%), and measured under high dynamic vacuum ($p \leq 3 \cdot 10^{-3}$ mbar). Around 400 °C, the sample started to sublimate.

Pair Distribution Function (PDF) Analysis

Total scattering measurements were performed using a *Stoe* Stadi-P diffractometer with Ag-Kα_1 radiation (λ = 0.55941 Å), a Ge(111) Johann monochromator, and a DECTRIS Mythen 1K detector in Debye-Scherrer geometry. The sample was loaded into a 1 mm inner diameter fused silica capillary (*Hilgenberg*), and five measurements were performed with heating using an *Oxford Cryostream* mounted vertically above the sample to temperatures of 20, 120, 225, 120, and 20 °C. Measurements were performed in three increments: 0.405-125.535°, 40.50-125.535°, and 81.0-125. 535° with a 0.405° step size, 110 s count time per step, doubling the counting time per step in the third range, and averaging the ranges together to improve the statistics at higher angles. Data were directly corrected for the 2θ offset of the instrument and polarization effects. Further correction and normalization of the 1D diffraction intensities were carried out to obtain the total scattering structure functions, $F(Q)$, which were Fourier transformed to obtain the PDF, $G(r)$ using PDFgetX3 within xPDFsuite.[7–10] The maximum value used in the Fourier transform of the total scattering data was 19.5 Å^{-1} with a Lorch modification function[11] applied to the $F(Q)$ data to minimize termination effects.

Structure models were generated from the parent structure (*Pnma*) using the software Isodistort,[12,13] and considering all rotational distortions in orthorhombic, monoclinic, and triclinic crystal systems. Refinements to the PDF data were performed using TOPAS v6.[14,15] A damping parameter (Q_{damp})[16,17] to account for instrumental *Q*-space resolution was refined to the 20 °C dataset and fixed for subsequent refinements. Corrections for the broadening and termination effects of Q_{max} truncation and broadening due to the Lorch function were fixed. All refinements of parent and subgroup structures further considered lattice parameters and rotational degrees of freedom of the $(SCN)^-$ anions allowed by the specific subgroup symmetry, a global scale factor, atomic displacement parameters for Li, S, C, and N, and a separate intramolecular displacement parameter for the $(SCN)^-$ anions.[18,19] Li and C site positions were fixed to their average positions to minimize the number of parameters in the model.

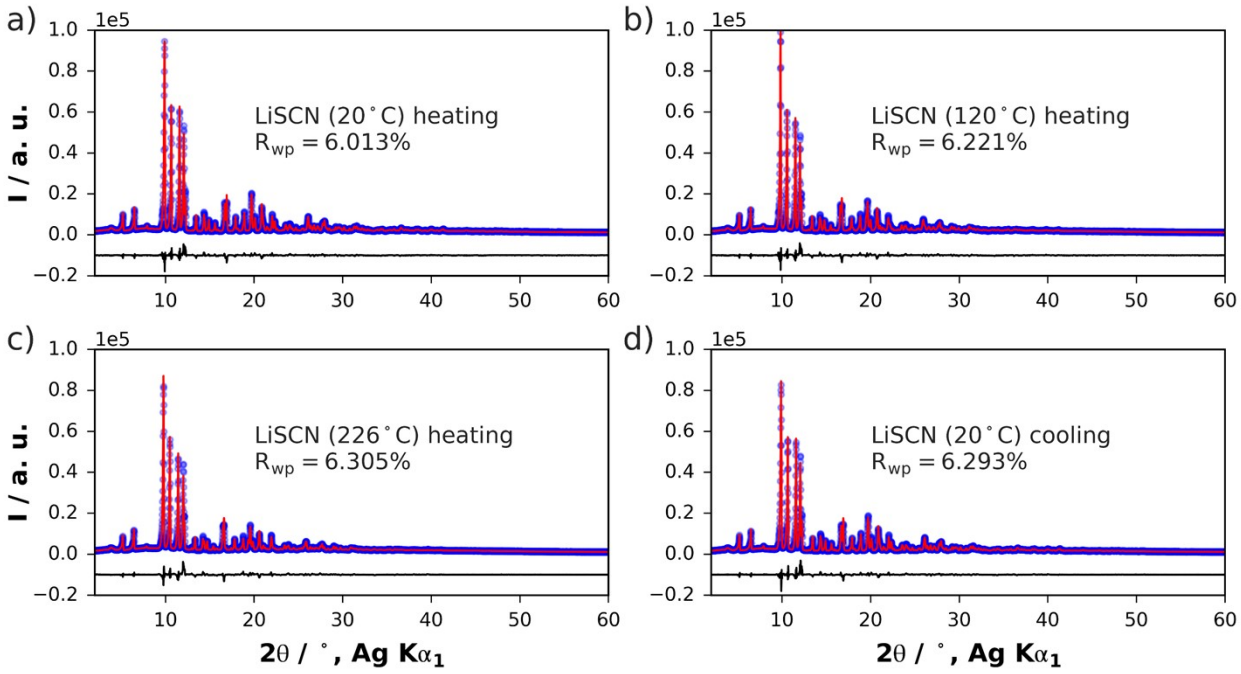

Figure S1: Rietveld refinements of the crystal structure with space group symmetry *Pnma* to the diffraction data at different temperatures. The observed (blue) and simulated (red) patterns are overlaid with their difference curve (black) plotted below. Refinements were performed in TOPAS v6.[14]

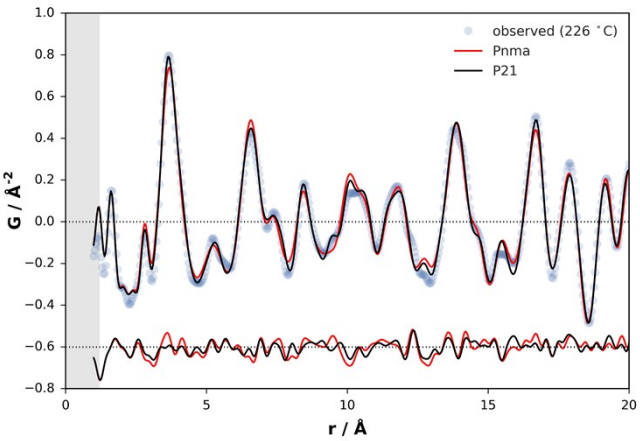

Figure S2: Exemplary results from real-space refinements of structure models to the PDF data. The simulated PDF and difference curve for the parent structure (*Pnma*, red curves) and a monoclinic subgroup (*P21*, black curves) are compared to the experimental data. The fits correspond to those referenced in Figure 7b and c.

Electrochemical Measurements

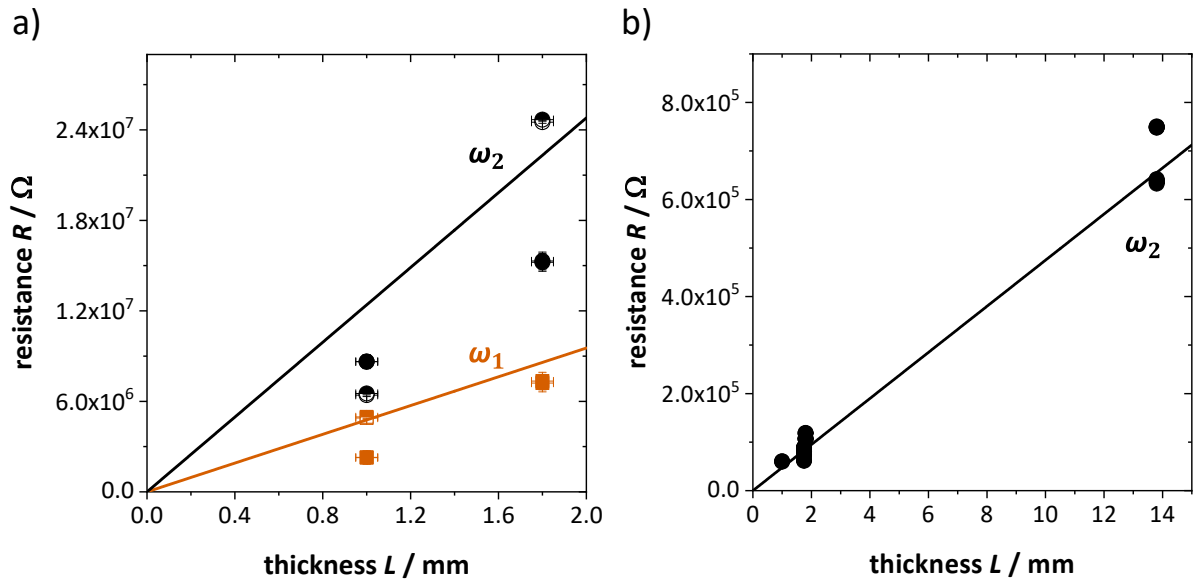

Figure S3: Resistance of anhydrous Li(SCN) as a function of sample thickness; a) T = 157-162 °C with the high frequency process (ω_1) in red squares and the low frequency process (ω_2) in black circles. Full symbols correspond to heating data; half-filled symbols correspond to cooling data. b) T = 239-243 °C, thickness scaling from several samples of anhydrous Li(SCN) showing the measured resistances corresponding to the low frequency process (ω_2).

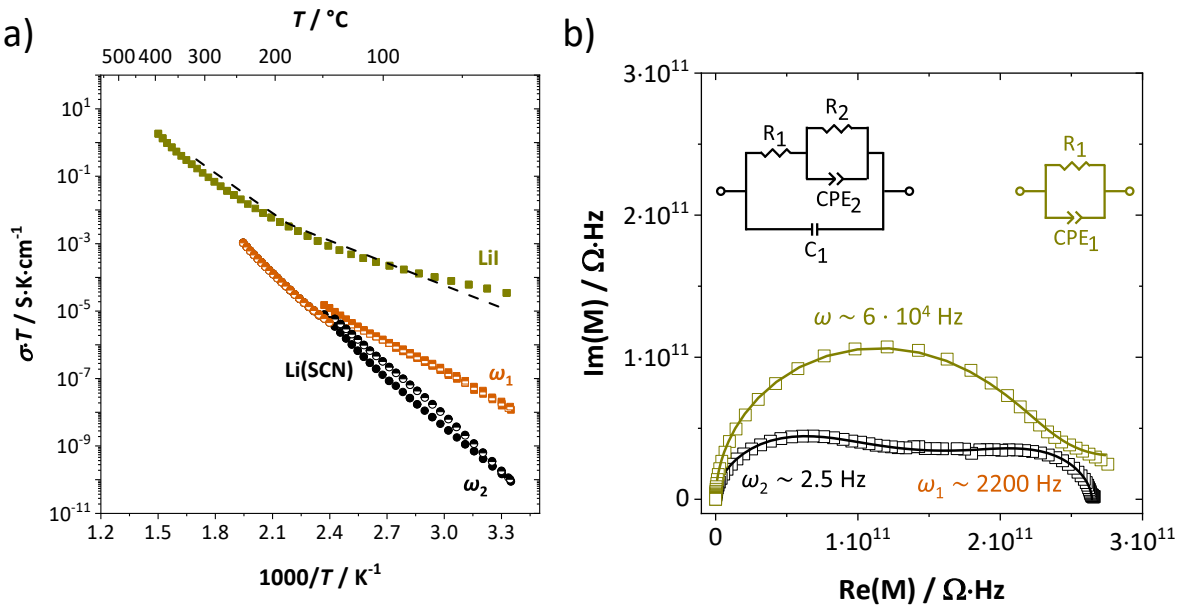

Figure S4: Impedance data for anhydrous Li(SCN) (black and red) and LiI (green). a) Arrhenius plot (dashed line corresponds to Poulsen, 1981).[20] The measured dielectric constant ε_r of LiI was around 30 for all temperatures. Full symbols are heating runs; half-filled symbols are cooling runs. b) Comparison of the complex modulus at 69 °C (Li(SCN)) and 66 °C (LiI).

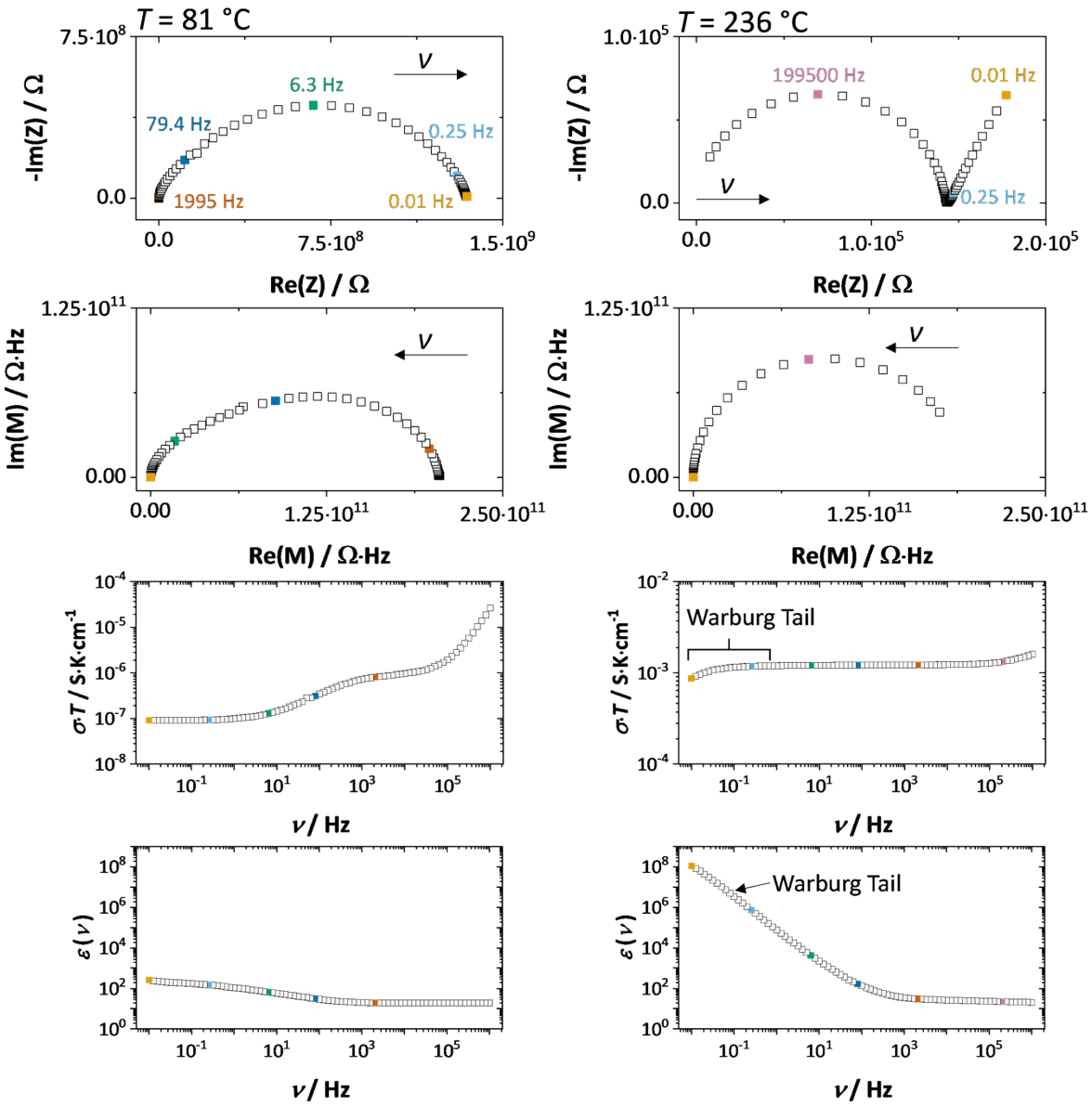

Figure S5: Impedance spectra for anhydrous Li(SCN) at intermediate temperatures (left 81 °C, right 236 °C) shown in different representations: complex impedance (first row), complex modulus representation (second row), frequency dependent conductivity (third row), and frequency dependent (apparent) dielectric constant (fourth row). Note that in the main text Figure 3 the angular frequency $\omega = 2\pi\nu$ was employed, while here the frequency ν was directly used.

As can be seen in Figure S5, at 81 °C it is obvious from the complex impedance signal that the frequency in the measured range is too low for the electrode polarization (Warburg diffusion tail) to be observed. Also the low frequency dielectric constant of about 100 is much too low for an electrode signal. Therefore, the electrode process cannot be observed at lower temperatures either. The Warburg tail, however, is clearly visible at 236 °C. The respective decrease in conductivity is also perceived in the conductivity vs. frequency presentation, and correspondingly the apparent dielectric constant rises above 100000. Overall, we conclude that at high frequencies we indeed observe two bulk signals, and did not erroneously

interpret Warburg response as bulk impedance signal. There is also no signal from blocking grain boundaries which would be expected between the bulk and electrode response.

Solid State NMR Literature Comparison

It is worth making a comparison to the investigations on $Na_3(PO_4)$,[21,22] which has been measured by ^{17}O, ^{23}Na and ^{31}P NMR. Around 310 °C $Na_3(PO_4)$ undergoes a phase transition to a high temperature phase (α-$Na_3(PO_4)$). Before this transition, the progression of observed ^{17}O and ^{23}Na NMR signals is very similar to observations made here for ^{15}N (main text, Figure 6) and ^{7}Li (Figure 4), respectively. With increasing temperature, an additional narrow signal develops, indicating a higher mobility as well as higher isotropy for the $(PO_4)^{3-}$ anion. A certain anisotropy of the signal is retained up to 252 °C, after which the signal becomes 100% isotropic and around 310 °C the phase transition occurs. This behavior is analogous to the one observed for Li(SCN), except that the anisotropy for $(SCN)^-$ is retained for the entire temperature range of ^{15}N measurements. In case of $Na_3(PO_4)$, the proposed model was that below 252 °C the anionic reorientation of $(PO_4)^{3-}$ occurs via a preferred C_3 axis (activation energy of (0.65 + 0.03) eV), and at higher temperatures the $(PO_4)^{3-}$ anion becomes completely rotationally disordered as in α-$Na_3(PO_4)$. Regarding Li(SCN), if we assume the change in magnetic shielding is (mostly) related to the anion motion, and presuming full $(SCN)^-$ anion rotation is possible, the mobility of the anion in the domain displaying the narrow isotropic signal is likely to be mainly linked to a fast local, nearly spherical rotation of the $(SCN)^-$ anion, and the broad anisotropic signal to quasi-stationary anions. Isotropic translational motions do probably contribute to a lesser degree.

References

1 M. Joos, M. Conrad, A. Rad, P. Kaghazchi, S. Bette, R. Merkle, R. E. Dinnebier, Th. Schleid and J. Maier, *submitted to Phys. Chem. Chem. Phys.*.

2 H. Henning, J. M. Bauchert, M. Conrad and Th. Schleid, *Z. Naturforsch.*, 2017, **72b**, 555–562.

3 K. MacKenzie and M. E. Smith, *Multinuclear Solid-State NMR of Inorganic Materials*, Pergamon, 1st edn., 2002.

4 D. C. Apperley, R. K. Harris and P. Hodgkinson, *Solid State NMR: Basic Principles and Practice*, Momentum Press, New York, 2012.

5 A. Bielecki and D. P. Burum, *J. Magn. Reson. Ser. A*, 1995, **116**, 215–220.

6 R. K. Harris, E. D. Becker, S. M. C. De Menezes, R. Goodfellow and P. Granger, *Solid State Nucl. Magn. Reson.*, 2002, **22**, 458–483.

7 P. Juhás, T. Davis, C. L. Farrow and S. J. L. Billinge, *J. Appl. Crystallogr.*, 2013, **46**, 560–566.

8 P. F. Peterson, E. S. Božin, T. Proffen and S. J. L. Billinge, *J. Appl. Crystallogr.*, 2003, **36**, 53–64.

9 S. J. L. Billinge and C. L. Farrow, *J. Phys. Condens. Matter*, 2013, **25**, 5.

10 X. Yang, P. Juhas, C. L. Farrow and S. J. L. Billinge, *arXiv:1402.3163*, 2014, 1–4.

11 E. Lorch, *J. Phys. C Solid State Phys.*, 1969, **2**, 229–237.

12 H. T. Stokes, D. M. Hatch and B. J. Campbell, ISODISTORT, ISOTROPY Software Suite, iso.byu.edu.

13 B. J. Campbell, H. T. Stokes, D. E. Tanner and D. M. Hatch, *J. Appl. Crystallogr.*, 2006, **39**, 607–614.

14 A. A. Coelho, *J. Appl. Crystallogr.*, 2018, **51**, 210–218.

15 A. A. Coelho, P. A. Chater and A. Kern, *J. Appl. Crystallogr.*, 2015, **48**, 869–875.

16 https://scripts.iucr.org/cgi-bin/paper?ko5004.

17 https://scripts.iucr.org/cgi-bin/paper?ib5055.

18 N. Rademacher, L. L. Daemen, E. L. Chronister and T. Proffen, *J. Appl. Crystallogr.*, 2012, **45**, 482–488.

19 D. Prill, P. Juhás, M. U. Schmidt and S. J. L. Billinge, *J. Appl. Crystallogr.*, 2015, **48**, 171–178.

20 F. W. Poulsen, *Solid State Ionics*, 1981, **2**, 53–57.

21 M. Witschas, H. Eckert, D. Wilmer, R. D. Banhatti, K. Funke, J. Fitter, R. E. Lechner, G. Korus and M. Jansen, *Z. Phys. Chem.*, 2000, **214**, 643.

22 M. Witschas, H. Eckert, H. Freiheit, A. Putnis, G. Korus and M. Jansen, *J. Phys. Chem. A*, 2001, **105**, 6808–6816.